

Article

AlGa_N-Delta-GaN Quantum Well for DUV LEDs

Cheng Liu ¹, Bryan Melanson ¹ and Jing Zhang ^{1,2,*}¹ Microsystems Engineering, Rochester Institute of Technology, Rochester, NY 14623, USA; cl7007@rit.edu (C.L.); bcm9356@rit.edu (B.M.)² Department of Electrical and Microelectronic Engineering, Rochester Institute of Technology, Rochester, NY 14623, USA

* Correspondence: jing.zhang@rit.edu

Received: 28 August 2020; Accepted: 28 September 2020; Published: 3 October 2020



Abstract: AlGa_N-delta-GaN quantum well (QW) structures have been demonstrated to be good candidates for the realization of high-efficiency deep-ultraviolet (DUV) light-emitting diodes (LEDs). However, such heterostructures are still not fully understood. This study focuses on investigation of the optical properties and efficiency of the AlGa_N-delta-GaN QW structures using self-consistent six-band *kp* modelling and finite difference time domain (FDTD) simulations. Structures with different Al contents in the Al_xGa_{1-x}N sub-QW and Al_yGa_{1-y}N barrier regions are examined in detail. Results show that the emission wavelength (λ) can be engineered through manipulation of delta-GaN layer thickness, sub-QW Al content (x), and barrier Al content (y), while maintaining a large spontaneous emission rate corresponding to around 90% radiative recombination efficiency (η_{RAD}). In addition, due to the dominant transverse-electric (TE)-polarized emission from the AlGa_N-delta-GaN QW structure, the light extraction efficiency (η_{EXT}) is greatly enhanced when compared to a conventional AlGa_N QW. Combined with the large η_{RAD} , this leads to the significant enhancement of external quantum efficiency (η_{EQE}), indicating that AlGa_N-delta-GaN structures could be a promising solution for high-efficiency DUV LEDs.

Keywords: deep-ultraviolet; light-emitting diodes; optical polarization; FDTD

1. Introduction

Ultraviolet (UV) light sources with emission wavelengths (λ) from 200 to 280 nm (UVC range) have been demonstrated to be the most efficient solution for surface/air/water sterilization [1–4]. Of all UV light sources, deep-UV (DUV) light-emitting diodes (LEDs) are the most promising option due to their compact size, fast response time, long lifetime, low power consumption, and environmental compatibility. However, cost and quantum efficiency issues currently impede DUV LEDs from completely replacing conventional DUV light sources such as mercury arc lamps. The III-Nitride materials used to fabricate DUV LEDs have been well studied and developed over the past 20 years. However, several challenges continue to limit the external quantum efficiency (η_{EQE}) of DUV LEDs to less than 10% [1,2,5], namely the lack of a native growth substrate, difficult p-type doping, and a large refractive index mismatch between the III–V semiconductor and air. The integration of advanced techniques, such as the use of a patterned sapphire substrate, multi-quantum barrier electron-blocking layers, and a highly reflective p-electrodes have allowed for the attainment of external quantum efficiencies of around 20%, as demonstrated at $\lambda = 278$ nm by Takano et al. in 2017 [6]. However, there is much room for the further improvement of overall device efficiency, especially in the active region. There are two main issues in the active region for AlGa_N-based DUV LEDs, the first being the quantum confined stark effect (QCSE), in which the large polarization fields in the epitaxial AlGa_N layers cause severe energy band bending which pushes the electron and hole wavefunctions to opposite sides of the QW, reducing the electron–hole recombination rate. Second, in a AlGa_N quantum well (QW) structure

with a high Al content, the crystal field split-off hole (CH) subband moves upwards and gradually reaches or bypasses the heavy hole (HH) and light hole (LH) subbands, which leads to dominant transverse-magnetic (TM)-polarized emission instead of transverse-electric (TE)-polarized emission. In addition, when the CH subband mixes with the HH and LH subbands, both TE- and TM-polarized recombination are reduced to much lower values [7,8]. In our previous study, we discuss the critical Al content at which emission becomes dominantly TM-polarized as well as the influence of the QW thickness on light polarization switching [8]. In addition to its impact on the recombination process, the optical polarization of emitted light also plays a critical role in light extraction efficiency [1]. Due to the interaction of the electric and magnetic field components of light, TM-polarized light prefers to propagate in the plane of the epitaxial layers, emitting from the edges of the device. The effective critical angle and escape cone for TM-polarized emission is extremely limited, making it difficult for TM-polarized light to escape from the top of planar LEDs. As a consequence, an extremely low η_{EXT} for TM-polarized light is observed from the top/bottom emitting LEDs, usually below 1%, which is much lower than the TE-polarized η_{EXT} between 10% and 20%.

Radiative recombination efficiency (η_{RAD}) can be improved through a reduction of the non-radiative recombination events [1] or through the improvement of the radiative recombination rate [9–11]. The non-radiative recombination rate is highly dependent on the dislocation density in the heterostructure, which can be significantly reduced by optimizing the substrate quality and growth technique. It has been reported that the internal quantum efficiency (η_{IQE}) can be boosted from 1% to 60% if the dislocation density is decreased from $1 \times 10^{10} \text{ cm}^{-2}$ to $5 \times 10^8 \text{ cm}^{-2}$ [1]. Recently, higher quality AlN and SiC substrates have been developed and used for the growth of DUV LEDs [12–16]. In contrast to substrate and growth optimization, few studies have focused on the engineering of the active region to reduce the both QCSE and tune the optical polarization of emitted light. Our previous work proposed an idea to solve this issue using AlGaIn-delta-GaN QWs [9]. Specifically, an ultra-thin delta-GaN layer is inserted into the AlGaIn QW center to form an AlGaIn/GaN/AlGaIn staggered heterostructure, which is embedded within AlN barriers. Similar InGaIn-delta-InN [17] and AlInN-delta-GaN [10] structures have also been developed for visible and DUV emission, respectively. There are several advantages to using an AlGaIn-delta-GaN QW over a conventional AlGaIn QW. First, the electron and hole wave function overlap is significantly improved through a reduction of the QCSE. Second, the insertion of delta-GaN layer serves to rearrange the valence band structure and ensures the HH subband sits above the LH and CH holes subbands at the Γ point, which leads to dominant TE-polarized emission. Third, large energy separation between the HH and CH valence subbands suppresses the band mixing effect and improves the rate of radiative conduction band to HH recombination. Due to these advantages, AlGaIn-delta-GaN QWs exhibit superior optical properties when compared with conventional AlGaIn square QWs [9].

Although encouraging results have been realized through reliable theoretical calculations, AlGaIn-delta-GaN QW structures have seen little experimental verification due to difficulties with the epitaxial growth of the structure. Thanks to the development in ultra-thin GaN growth processes [18–22], we successfully grew and fabricated AlN-delta-GaN QW UV LEDs with emission wavelengths of $\lambda = 234, 246$ and 298 nm , which can be approximated as high Al-content AlGaIn-delta-GaN QWs [23,24]. A custom polarization-dependent electroluminescence (EL) measurement setup was built to study the polarization properties of the light emitted from the grown structures. Results show that all three LEDs exhibit TE-dominant emission, confirming our theoretical calculations.

In addition, we continued to pursue the design of improved AlGaIn-delta-GaN QW epitaxial structures. In our current design, AlN barrier layers surround the $\text{Al}_{0.9}\text{Ga}_{0.1}\text{N}$ -delta-GaN active region, with the delta-GaN layer having a thickness of 5 \AA . This epitaxial stack was grown on an AlN/sapphire substrate with a dislocation density of 10^{10} cm^{-2} using a Veeco Gen10 molecular beam epitaxy (MBE) system [25,26]. Long and streaky reflection high-energy electron diffraction (RHEED) patterns and smooth atomic force microscope (AFM) images indicate a smooth surface after completion of the growth process. X-ray diffraction patterns and cross-sectional transmission electron microscopy images

confirm the formation of a two monolayer (ML) delta-GaN layer in the center of the active region. More growth and characterization details can be found in [25,26]. The optical properties from this structure were also examined in the previous study, showing up to 85% η_{IQE} at $\lambda = 255$ nm, which is very promising for DUV LEDs, especially considering that structure was grown on a conventional AlN template [26].

Although tremendous progress has been made, there are still several issues remaining which obstruct the development of efficient DUV LEDs based on AlGaIn-delta-GaN QW active regions. To have a better understanding of the proposed structure, the physics from the AlGaIn-delta-GaN QWs with different Al contents in the $\text{Al}_x\text{Ga}_{1-x}\text{N}$ sub-QW and $\text{Al}_y\text{Ga}_{1-y}\text{N}$ barrier regions require further investigation. In addition, the η_{EXT} of AlGaIn-delta-GaN QW-based DUV LEDs need to be studied to allow for the attainment of high η_{EQE} . In this study, we examined the physics and optical properties of AlGaIn-delta-GaN active regions with differing delta-GaN thickness, barrier Al content, and QW Al content using a self-consistent six-band $k\cdot p$ model. Finite difference time domain (FDTD) simulations were also used to investigate the light radiation properties and η_{EXT} of AlGaIn-delta-GaN QW LEDs emitting between $\lambda = 230$ nm and $\lambda = 280$ nm and compare them to those of conventional AlGaIn QW LEDs. Results show large enhancements in light extraction efficiency (η_{EXT}) through use of AlGaIn-delta-GaN QWs which emit primarily TE-polarized light, which is easier to extract into free space.

2. Materials and Methods

The optical properties of the AlGaIn-delta-GaN QWs were calculated using a self-consistent 6-band $k\cdot p$ model which considers the effects of spontaneous and piezoelectric polarization electric fields, strain, and carrier screening. More details of the model can be found in references [27–30]. The simulated structures, including a conventional AlGaIn QW and the proposed AlGaIn-delta-GaN QW, have a 6 nm fixed width barrier layer on each side of the QW structure. AlN is used as the substrate for all calculations. For the conventional AlGaIn QW, the QW thickness is fixed at 3 nm for a fair comparison. For the AlGaIn-delta-GaN QW, we focused only on a structure with a symmetric design, which had a delta-GaN QW layer embedded between two 1.5 nm AlGaIn sub-QW layers, as shown in Figure 1a. Note that the band structure parameters such as deformation energy have large variability which strongly influences the energy band lineups and profiles. The parameters used in this study and listed in Table 1 are taken from references 27 and 31 and have been widely used to study the fundamental physics of III-Nitride-based devices. The carrier density n is fixed at $n = 5 \times 10^{18} \text{ cm}^{-3}$ for all calculations.

Three-dimensional FDTD simulations were performed to investigate the η_{EXT} of bottom emitting DUV LEDs on sapphire substrates emitting between $\lambda = 230$ nm and $\lambda = 280$ nm using Synopsys Fullwave [32]. Both TE and TM polarizations were investigated in our study. Rsoft Fullwave solves Maxwell's equations in the time domain to allow for a much higher accuracy than ray tracing approaches, which neglect phenomena such as thin film interference and mode coupling. As shown in Figure 1b, the structure used for simulations consists of an AlN on sapphire substrate, a 100 nm n-AlGaIn layer, a 50 nm multiple quantum well (MQW) region, a 25 nm p-AlGaIn layers, and a 20 nm p-GaN contact layer. Since UV LEDs are usually packaged in a flip-chip configuration, with light generated within the MQW region emitted through the sapphire substrate, our simulation structure inverts the orientation of the epitaxial layers to mimic this orientation in a "bottom emitting" configuration.

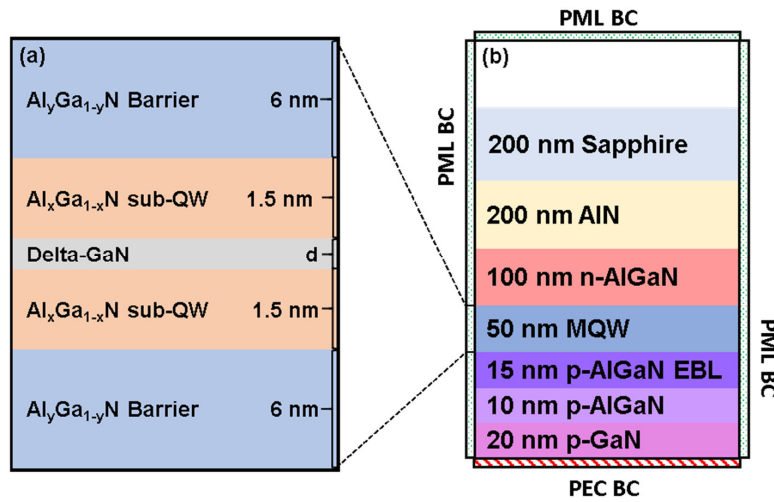


Figure 1. (a) Schematic of the AlGaN-delta-GaN structure studied in this work. The barrier thickness is fixed at 6 nm and the sub-QW thickness is 1.5 nm on each side of the delta-GaN layer. (b) Cross-sectional representation of the three-dimensional structure used for the finite difference time domain (FDTD) simulation. Perfectly matched layer (PML) and perfect electric conductor (PEC) boundary conditions (BC) are shown at the domain surfaces, MQW stands for multiple quantum well.

Table 1. Material parameters for GaN and AlN [27].

Parameter	GaN	AlN
a (Å) at $T = 300$ K	3.189	3.112
c (Å) at $T = 300$ K	5.185	4.982
E_g (eV) at $T = 300$ K	3.437 [31]	6.16 [31]
Δ_{cr} (eV)	0.010	−0.227
Δ_{so} (eV)	0.017	0.036
m_e^{\parallel} / m_0	0.21	0.32
m_e^{\perp} / m_0	0.20	0.30
A1	−7.21	−3.86
A2	−0.44	−0.25
A3	6.68	3.58
A4	−3.46	−1.32
A5	−3.40	−1.47
A6	−4.90	−1.64
D1 (eV)	−3.6	−2.9
D2 (eV)	1.7	4.9
D3 (eV)	5.2	9.4
D4 (eV)	−2.7	−4.0
C11 (GPa)	390	396
C12 (GPa)	145	137
C13 (GPa)	106	108
C33 (GPa)	398	373
d13 (pm/V)	−1.0	−2.1
d33 (pm/V)	1.9	5.4

The size of the simulation domain was set to be 5 μm in width and length, and 1.6 μm in height in order to optimize the simulation convergence and simulation run time. A non-uniform 3D mesh with cell dimensions between 1 and 5 nm was used. Although a UV LED epi-stack would be grown on a sapphire substrate at least 200 μm thick, simulating such a device with an acceptable degree of accuracy using direct solution of Maxwell’s equations would require significant simulation time, so a 200 nm-thick sapphire was used here. Use of a growth substrate of significantly reduced thickness is common practice when performing an FDTD simulation of LEDs as it allows for an order of magnitude reduction in the simulation run time while maintaining the accuracy of the simulation [33–35]. Table 2 lists the refractive index (n) and extinction coefficient (k) of the materials used in this study. Refractive index values for all materials were taken from Palik et al. [36] while the Al contents for each layers were selected based on the reported values [1]. Vegard’s law was employed here to determine the refractive index of AlGaIn material at a specific wavelength.

Table 2. Refractive index (n) and extinction coefficient (k) of the materials [36].

GaIn		AlIn		Sapphire		Electron Blocking Layer (EBL)			
λ	n	k	n	k	n	k	Al Content	n	k
230	2.756	0.6176	2.499	0.0275	1.865	−0.026	0.97	0.022	2.507
240	2.699	0.5593	2.441	0.0220	1.855	−0.019	0.96	0.0096	2.451
250	2.657	0.5188	2.396	0.0191	1.845	−0.016	0.95	0.008	2.410
260	2.626	0.4886	2.362	0.0161	1.837	−0.010	0.94	0.0062	2.378
270	2.604	0.4644	2.334	0.0118	1.830	−0.004	0.93	0.0043	2.353
280	2.589	0.4435	2.312	0.0089	1.824	−0.001	0.92	0.0022	2.334
p/n/Barrier-AlGaIn				Quantum Well (QW) AlGaIn			Active Region		
λ	Al Content	n_1	k	Al Content	n_2	k	$n = (n_1 + n_2)/2$		
230	0.86	2.535	0.0640	0.77	2.558	0.124	2.546		
240	0.8	2.492	0.0477	0.70	2.518	0.078	2.505		
250	0.76	2.459	0.0318	0.63	2.493	0.149	2.476		
260	0.72	2.436	0.0248	0.55	2.481	0.128	2.458		
270	0.68	2.421	0.0107	0.48	2.474	0.204	2.448		
280	0.64	2.412	0.0067	0.41	2.475	0.201	2.444		

A perfect electric conductor (PEC) boundary condition was used at the bottom of the simulation domain in place of a reflective p-metal contact, while perfectly matched layer (PML) boundary conditions were used for all other domain surfaces. To measure the η_{EXT} of a given structure, a three-dimensional power monitor box was positioned to enclose a dipole source located at the center of the active region and simulation domain and measure its luminous power flux [33]. Another two-dimensional monitor was located at the top of the simulation domain, 1 μm above the sapphire surface, to measure the luminous power flux passing through the sapphire-air interface. By calculating the ratio of the luminous power flux through these two monitors over the course of each simulation run, we were able to determine the fraction of light emitted by the dipole source which successfully escapes across the sapphire–air interface into free space. The monitor at the top of the simulation domain also served to record the spatial intensity of incident radiation, allowing for the generation of far field intensity plots and the determination of the angular distribution of light escaping across the sapphire–air interface. Additional two-dimensional monitors were placed vertically within the simulation domain to record the spatial electric field intensity to allow for the further characterization of the angular distribution of light within different regions of the simulated structures.

3. Results and Discussion

3.1. Physics of AlGa_xN-Delta-GaN QW Designs with Different Sub-QW and Barriers

As introduced previously, promising results such as extremely high 85% η_{IQE} have been achieved from MBE-grown Al_{0.9}Ga_{0.1}N-delta-GaN structures with 5 Å delta-GaN layer thickness at ~255 nm. However, in order for AlGa_xN-delta-GaN QW structures to be suitable for widespread implementation in DUV LEDs, their emission wavelength should be easily adjustable through the alteration of the Al content in the Al_xGa_{1-x}N sub-QW and Al_yGa_{1-y}N barrier regions without sacrificing their characteristic high efficiencies. This work extends our study of the physics of AlGa_xN-delta-GaN QWs to structures with different sub-QW and barrier designs. For example, by reducing the Al content (x) in the Al_xGa_{1-x}N sub-QW, the emission wavelength redshifts due to a reduction in the effective bandgap, which is determined by both the delta-GaN layer thickness and Al content (x) in the Al_xGa_{1-x}N sub-QW. Our previous study reported peak emission wavelengths of $\lambda = 253.6$ nm from an Al_{0.7}Ga_{0.3}N-delta-GaN QW structure and $\lambda = 245.1$ nm from an Al_{0.8}Ga_{0.2}N-delta-GaN QW. Both structures had a delta-GaN thickness of $d = 3$ Å. More Al contents in Al_xGa_{1-x}N sub-QW are studied here and plotted in Figure 2a. Different delta-GaN layer thicknesses (d) of 3 Å, 4 Å, and 5 Å were all considered. In general, the emission wavelength decreases as the Al content x increases due to the widening of the effective bandgap as more Al is incorporated into the sub-QW, which is consistent with the results of our previous study. Specifically, for the AlGa_xN-delta-GaN QW with a 5 Å delta-GaN layer, the emission wavelength can be varied from $\lambda = 278$ nm to $\lambda = 261$ nm by increasing the sub-QW Al content from 60% to 80%. Moreover, $\lambda = 252$ –269 nm and $\lambda = 243$ –261 nm ranges can likewise be achieved using 4 Å and 3 Å delta-GaN layers, respectively. Note that there are wavelength overlaps between the three ranges, allowing for flexibility in the design of AlGa_xN-delta-GaN QW structures and the targeting of precise emission wavelengths. For example, to achieve $\lambda = 262$ nm emission, one could use Al_{0.61}Ga_{0.39}N-delta-GaN QW with 3 Å delta-GaN, Al_{0.68}Ga_{0.32}N-delta-GaN QW with 4 Å delta-GaN, or Al_{0.78}Ga_{0.22}N-delta-GaN QW with 5 Å delta-GaN, as highlighted in Figure 2a.

In addition to the Al content in the sub-QW, the physics of the AlGa_xN-delta-GaN QW structures with different Al contents (y) in the Al_yGa_{1-y}N barrier were also investigated in this study. As y increases from 0.6 to 1, the magnitudes of the electrostatic fields in both the barriers and sub-QWs increase, as shown in Figure 2b, which leads to severe band bending in structures with high Al-content AlGa_xN barriers. Figure 2c,d compare the band structures and wave function positions of Al_{0.5}Ga_{0.5}N-delta-GaN QW structures with Al_{0.6}Ga_{0.4}N and AlN barriers, respectively. The large electrostatic field in the structure with an AlN barrier causes heavy band bending, which exacerbates the QCSE and reduces the electron–hole wavefunction overlap, leading to a degradation in the optical properties and efficiency of this design. On the other hand, for the Al_{0.6}Ga_{0.4}N barrier structure, band bending is significantly reduced, increasing the wavefunction overlap significantly.

In our previous work, we found that the emission wavelength can be engineered by altering the thickness of the delta-GaN layer. More specifically, $\lambda \sim 254$, 276 and 293 nm can be achieved using delta-GaN thicknesses of $d = 3$ Å, 6 Å, and 9 Å, respectively, for a Al_{0.7}Ga_{0.3}N-delta-GaN QW structure [9]. However, only certain wavelengths can be achieved by changing the delta-GaN layer thickness. Here, we present an alternate solution for manipulating the emission wavelength of AlGa_xN-delta-GaN QW structures. Figure 2a indicates that tuning the sub-QW Al content (x) can adjust the wavelength. Figure 3 plots the wavelength distribution for AlGa_xN-delta-GaN QWs with different sub-QW and barrier Al contents. The delta-GaN thickness is fixed at $d = 3$ Å for these calculations. By varying the Al content in the sub-QW and barrier regions, the emission wavelength can be tuned from $\lambda = 235$ nm to $\lambda = 291$ nm for the structure with a 3 Å delta-GaN layer, which is much wider than the range possible by adjusting only the sub-QW Al content. In general, the emission wavelength is shown to decrease with decreasing barrier Al content. This can be attributed to a reduction in the polarization field for a lower Al content barrier designs.

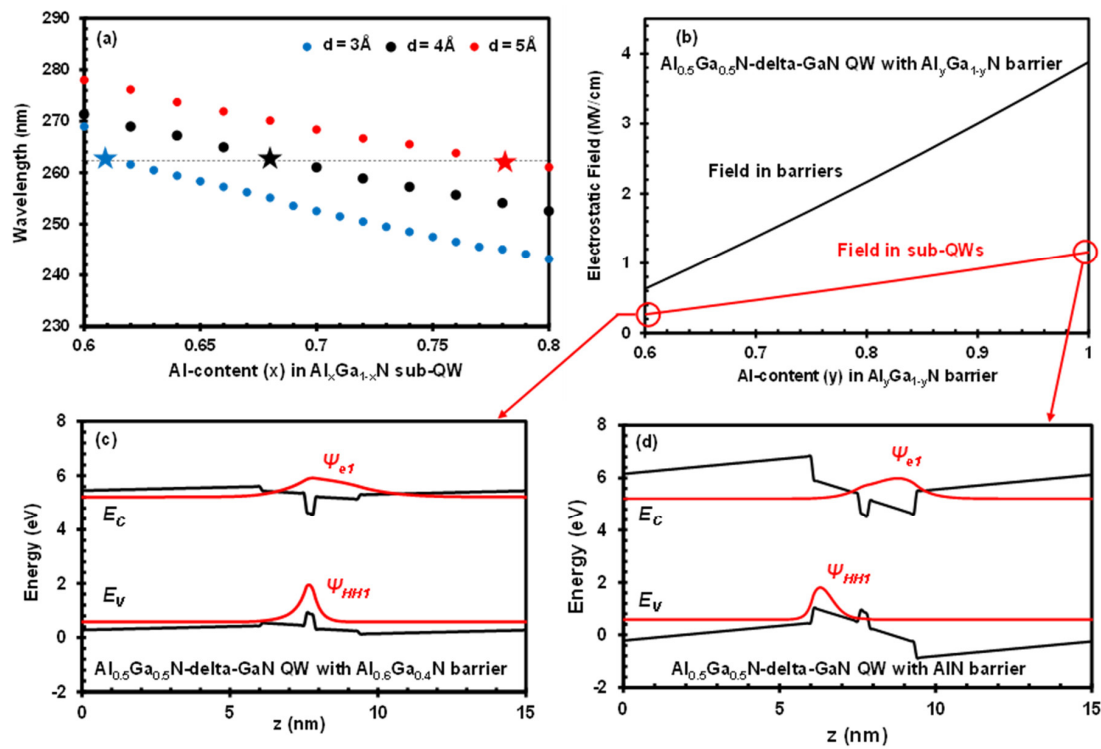


Figure 2. (a) Emission wavelengths from Al_xGa_{1-x}N-delta-GaN QW/AlN barrier with different sub-QW Al contents ($x = 0.6-0.8$) and delta-GaN thicknesses ($d = 3-5 \text{ \AA}$); (b) electrostatic fields in barriers and sub-QWs from Al_{0.5}Ga_{0.5}N-delta-GaN QWs with $d = 3 \text{ \AA}$. Band structure and wave function of Al_{0.5}Ga_{0.5}N-delta-GaN QW with (c) the Al_{0.6}Ga_{0.4}N barrier and (d) the AlN barrier.

To investigate the optical properties of AlGa_N-delta-GaN structures, spontaneous emission radiative recombination rates per unit volume (R_{sp}) were calculated. Figure 4a shows the corresponding R_{sp} for the AlGa_N-delta-GaN QWs whose emission wavelengths were shown in Figure 3. The R_{sp} drops significantly as the Al content difference between the QW and barrier increases, which can be attributed to strengthening the polarization electric field in the active region due to an increase in the lattice mismatch-induced strain. However, although R_{sp} decreases with increasing barrier Al content, even high-Al-content structures maintain R_{sp} in excess of $> 1 \times 10^{26} \text{ s}^{-1}\text{cm}^{-3}$. As a comparison, the R_{sp} values for conventional 3 nm AlGa_N QWs were calculated and plotted in Figure 4b as a function of emission wavelength. The conventional AlGa_N QW exhibits low R_{sp} values of around $1 \times 10^{25} \text{ s}^{-1}\text{cm}^{-3}$ throughout the DUV range from $\lambda = 230 \text{ nm}$ to $\lambda = 280 \text{ nm}$, due to the severe manifestation of the QCSE. In contrast, by carefully engineering the Al content of the barrier and sub-QW regions, an R_{sp} of around $4 \times 10^{26} \text{ s}^{-1}\text{cm}^{-3}$ can be maintained for the AlGa_N-delta-GaN QW structure, an enhancement of 40 times when compared with a conventional AlGa_N QW emitting between $\lambda = 230 \text{ nm}$ and $\lambda = 280 \text{ nm}$. It is noteworthy that the R_{sp} of the conventional AlGa_N QW increases up to $3 \times 10^{25} \text{ s}^{-1}\text{cm}^{-3}$ at an emission wavelength of $\lambda = 230 \text{ nm}$, however, the vast majority of the photons generated by this structure at $\lambda = 230 \text{ nm}$ are TM-polarized and difficult to extract from the LED structure into free space.

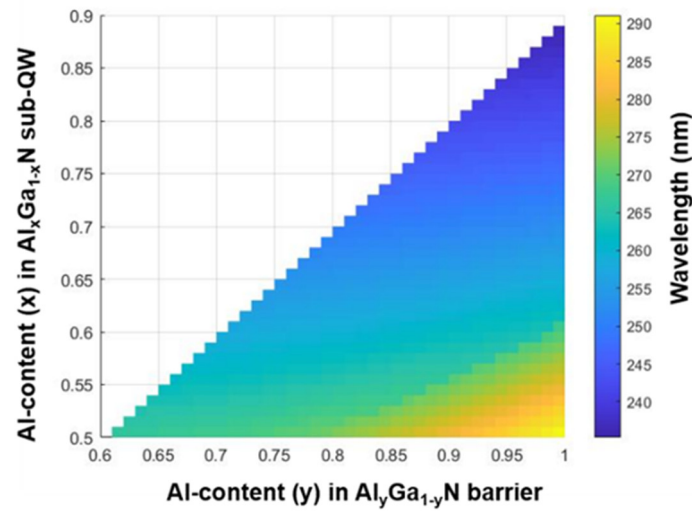


Figure 3. Wavelength color map for a 3 Å AlGaIn-delta-GaN QW with different sub-QWs and barrier Al contents.

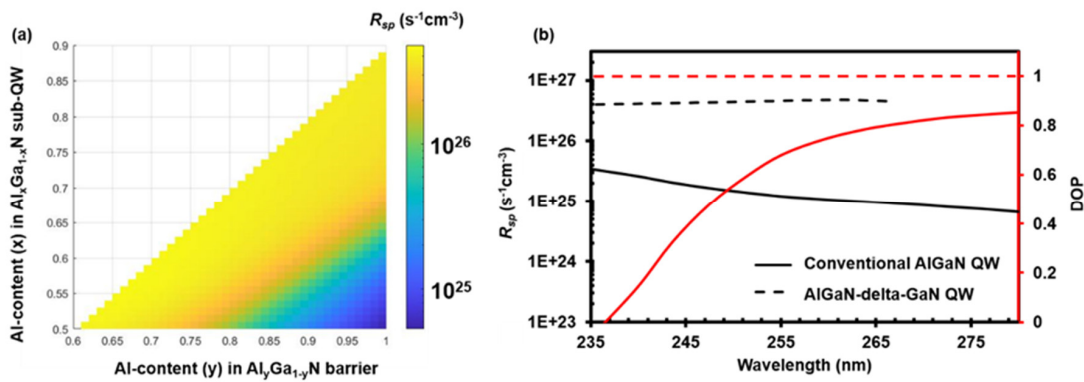


Figure 4. (a) Spontaneous emission rate color map for a 3 Å AlGaIn-delta-GaN QW with different sub-QW and barrier compositions. Band structure and wave function of $Al_{0.5}Ga_{0.5}N$ -delta-GaN QW with (b) R_{sp} values from conventional AlGaIn QW (solid line) and the highest R_{sp} value from AlGaIn-delta-GaN QW (dash line) at different wavelengths; red line plots the degree of polarization (DOP) from the conventional AlGaIn QW.

Another advantage of the AlGaIn-delta-GaN QW design over conventional AlGaIn QWs, as discussed in our previous study [9], is to ensure dominant TE-polarized emission. Because the presence of the delta-GaN layer ensures a dominant conduction band to HH recombination and a large energy separation between the HH and CH subbands, the vast majority of emitted light have TE polarization for all AlGaIn-delta-GaN QW designs. Therefore, the degree of polarization (DOP), which is defined as $p = \frac{I_{TE} - I_{TM}}{I_{TE} + I_{TM}}$, is near unity for all AlGaIn-delta-GaN structures, regardless of barrier and sub-QW composition. On the other hand, for conventional AlGaIn QWs, small or even negative DOP values are observed, indicating dominant TM-polarized emission, especially for shorter wavelengths. Because TM-polarized light is difficult to extract from both the top and bottom of planar LED devices, the η_{EQE} of conventional AlGaIn QWs is extremely poor, making AlGaIn-delta-GaN QW designs a promising high efficiency alternative.

3.2. Efficiencies of AlGaIn-delta-GaN QWs

To further demonstrate the superior optical properties of AlGaIn-delta-GaN QW in terms of efficiency, the calculated R_{sp} values were used to derive η_{RAD} based on the equation

$\eta_{RAD} = R_{sp} / (A \cdot n + R_{sp} + C \cdot n^3)$ [1]. Shockley–Read–Hall (SRH) coefficient (A) values, which generally range from 1×10^6 to $1 \times 10^{10} \text{ s}^{-1}$, are strongly influenced by the threading dislocation density in the heterostructure. In this study, an A value of $1 \times 10^7 \text{ s}^{-1}$ was used for all η_{RAD} calculations [37]. The Auger coefficient (C) is usually ignored for LED applications. Here, we used a C value of $1 \times 10^{33} \text{ cm}^6/\text{s}$ [37], which is consistent with the values reported and calculated in the literature. Figure 5 plots the η_{RAD} from $\text{Al}_{0.5}\text{Ga}_{0.5}\text{N}$ -delta-GaN QWs with $\text{Al}_x\text{Ga}_{1-x}\text{N}$ ($x = 0.6\text{--}1$) barriers. The large R_{sp} value of $4.54 \times 10^{26} \text{ s}^{-1}\text{cm}^{-3}$ from the structure with the $\text{Al}_{0.6}\text{Ga}_{0.4}\text{N}$ barriers leads to an extremely high η_{RAD} of 90%. As the Al content in the barrier increases, the R_{sp} value drops below $1 \times 10^{25} \text{ s}^{-1}\text{cm}^{-3}$, which corresponds to the low η_{RAD} of 10%. As mentioned previously, by correctly selecting Al contents in both sub-QW and barrier, a large R_{sp} value can be maintained over the entire emission range from $\lambda = 230 \text{ nm}$ to $\lambda = 280 \text{ nm}$. This can allow for the attainment of 90% η_{RAD} , which is comparable or higher to the reported values over nearly the entire DUV range [21,38–45]. It has been demonstrated that by reducing the dislocation density from $1 \times 10^{10} \text{ cm}^{-2}$ to $5 \times 10^8 \text{ cm}^{-2}$, the η_{IQE} can be improved from 1% to 60% for the conventional AlGaIn QW structure [1]. It is highly likely that by using higher quality, lower defect density substrates, the η_{RAD} of AlGaIn-delta-GaN QW structures can likewise be enhanced, possibly to near 100%. In addition to η_{RAD} , the carrier lifetime can also be estimated using R_{sp} data based on the equation $\tau = (A \cdot n + R_{sp} + C \cdot n^3) / n$. Results show a low 10 ns radiative carrier lifetime from the AlGaIn-delta-GaN QW, which is much smaller than that of a conventional AlGaIn QW (~1000 ns) calculated by the values in Figure 4b.

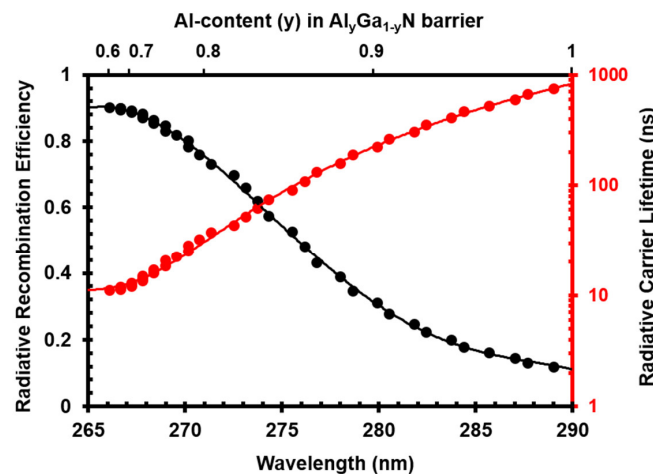


Figure 5. Radiative recombination efficiency (black) and radiative carrier lifetime (red) from a $\text{Al}_{0.5}\text{Ga}_{0.5}\text{N}$ -delta-GaN QW with different barrier Al content; the delta-GaN layer thickness is fixed at 3 Å.

To study the light extraction properties from DUV LEDs, we consider both TE- and TM-polarized emission. Here, the TE-polarized light is defined light which has its electric field component perpendicular to the growth direction (c axis) while the TM-polarized light has an electric field component parallel to the growth direction. Figure 6a plots the polarized light extraction efficiencies for typical LEDs between $\lambda = 230 \text{ nm}$ and $\lambda = 280 \text{ nm}$. In general, both TE- and TM-polarized η_{EXT} have low values due to the large refractive index difference between the semiconductor and air. However, the TM-polarized photons are even more difficult to extract from the top/bottom of the device because of their natural emission shape inside the active region. As a consequence, a η_{EXT} of less than 1% is observed for TM-polarized photons between 230 nm and 280 nm. Although TE-polarized photons have a relatively large η_{EXT} , generally between 10% and 20%, the TM-polarized photons generated in the active region still serve to lower the overall η_{EXT} . Different η_{EXT} values at different wavelengths can be attributed to the light propagation profiles variation caused by the different refractive index for each structure, as well as the absorption difference. Here, we introduce the concept of “effective” η_{EXT} , which considers both the extraction efficiency of TE and TM-polarized components, as well as

the degree of polarization of the structure at a certain wavelength, in order to study the practical light extraction behavior of DUV LEDs. As shown in Figure 6a, the effective η_{EXT} for the conventional AlGaIn QW is almost identical to the TE-polarized η_{EXT} at longer emission wavelengths ($\lambda = 270$ nm to $\lambda = 280$ nm) because the majority of the photons generated in the active region are TE-polarized. However, at shorter emission wavelengths, especially around $\lambda \sim 230$ nm, more TM-polarized photons are generated, which rarely contribute little to the total light output of the device as they are much more difficult to extract. As a result, only 7% η_{EXT} is realized for the conventional AlGaIn QW at $\lambda = 230$ nm, around half that of the TE-polarized η_{EXT} . In contrast, for an AlGaIn-delta-GaN QW structure, almost all emission is TE-polarized even at shorter emission wavelengths, enabling high effective extraction efficiencies across the entire DUV range and reducing the need for additional extraction enhancement methods, such as surface roughening or the formation of photonic crystals or nanowires.

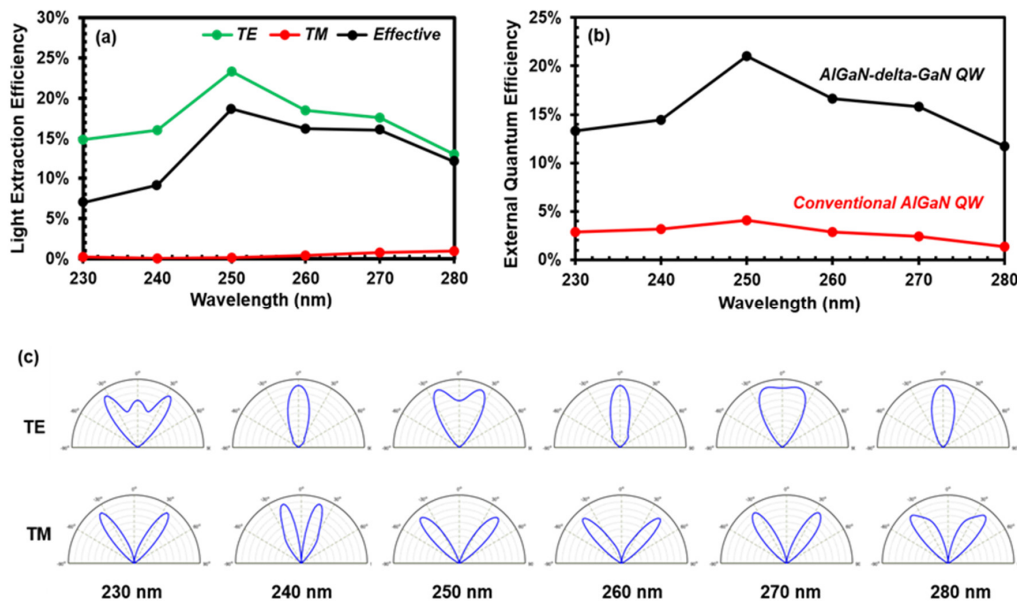


Figure 6. (a) TE-polarized η_{EXT} (green), TM-polarized η_{EXT} (red), and effective η_{EXT} (black) from the conventional DUV LEDs at different wavelengths and (b) η_{EQE} from conventional AlGaIn QW (red) and the AlGaIn-delta-GaN QW (black); (c) polarized far field patterns from DUV LEDs at different emission wavelengths.

Assuming that the injection efficiencies from all the DUV LED structures are 100%, the total η_{EQE} can be calculated based on the η_{RAD} and effective η_{EXT} collected previously, and is plotted in Figure 6b. For the conventional AlGaIn QW, the total η_{EQE} is limited to less than 4% due to low η_{RAD} and low η_{EXT} caused by difficult to extract TM-polarized photons. For AlGaIn-delta-GaN QWs, for which η_{RAD} is much higher throughout the DUV emission range ($\lambda = 230$ nm to $\lambda = 280$ nm), η_{EQE} is determined primarily by the effective η_{EXT} , which ranges between 12% and 21%. Here, we used 90% η_{RAD} for the AlGaIn-delta-GaN QW at all wavelengths, which was obtained through the engineering of the active region, as discussed previously. The current record η_{EQE} from a DUV LED without encapsulation is 16.1%, reported for a device emitting at $\lambda = 278$ nm and utilizing a patterned sapphire substrate, a highly reflective p-electrode, and a transparent p-AlGaIn layer to improve η_{EXT} with no improvements to the active region [6]. By integrating our AlGaIn-delta-GaN QW structure with these other methods of improving η_{EXT} it is quite possible that record high efficiencies could be realized, making DUV LEDs much more suitable replacements for conventional UV light sources. In addition to external quantum efficiency enhancement, AlGaIn-delta-GaN QWs could also improve the light emission profile. Figure 6c plots the polarized far field patterns from DUV LEDs at different wavelengths ($\lambda \sim 230$ – 280 nm). In general, TE-polarized light has a Lambertian radiation pattern while TM-polarized light presents a “rabbit-ear” pattern. For shorter emission wavelengths around 230 nm,

conventional AlGaIn QWs emit a significant amount of TM-polarized light, leading to a “rabbit-ear” pattern, in which the majority of the light escapes into free space at high angles from the surface normal. In contrast, the AlGaIn-delta-GaN QW ensures the dominant TE-polarized emission and therefore the Lambertian shape, which is more desirable for LED applications.

4. Conclusions

In conclusion, this work extends the study of the AlGaIn-delta-GaN QW designs by investigating the physics and efficiency of structures with different Al contents in $\text{Al}_x\text{Ga}_{1-x}\text{N}$ sub-QW and $\text{Al}_y\text{Ga}_{1-y}\text{N}$ barrier regions. It was found that the electrostatic field becomes larger as the barrier Al content increases, worsening the QCSE and red-shifting the emission wavelength. Further investigation of the structure revealed that the emission wavelength of AlGaIn-delta-GaN QWs can be adjusted through the engineering of the sub-QW Al content, barrier Al content, and the delta-GaN layer thickness while maintaining high R_{sp} and an η_{IQE} of around 90% over the entire DUV range. In general, structures with a smaller Al content difference between barrier and sub-QW region show a larger spontaneous emission rate due to the reduced strain effects and polarization electric field intensities. Compared to conventional AlGaIn QWs, R_{sp} enhancements of up to 40 times were realized for AlGaIn-delta-GaN QW structures. In addition, the use of AlGaIn-delta-GaN QW structures ensures the minimal emission of TM-polarized light, improving the effective η_{EXT} . The EQE calculated using the radiative recombination efficiencies generated by six-band $k \cdot p$ calculations and the light extractions efficiencies taken from the FDTD simulations for AlGaIn-delta-GaN QWs emitting between 230 nm and 280 nm ranges between 12% and 21%. These values are 3 to 7 times higher than those of conventional AlGaIn QWs emitting over the same wavelength range. These results show that AlGaIn-delta-GaN QW structures could be promising alternatives to conventional AlGaIn QWs for the development of record high-efficiency DUV LEDs.

Author Contributions: Conceptualization, C.L. and J.Z.; methodology, C.L. and B.M.; software, C.L. and B.M.; validation, C.L., B.M. and J.Z.; formal analysis, C.L. and B.M.; investigation, C.L.; resources, J.Z.; writing—original draft preparation, C.L.; writing—review and editing, B.M. and J.Z.; supervision, J.Z.; funding acquisition, J.Z. All authors have read and agreed to the published version of the manuscript.

Funding: This research was funded by the Office of Naval Research under Award No. N00014-16-1-2524, and the National Science Foundation (NSF) under Award No. ECCS 1751675.

Conflicts of Interest: The authors declare no conflict of interest.

References

1. Kneissl, M.; Rass, J. *III-Nitride Ultraviolet Emitters*; Springer: Cham, Switzerland, 2016; Volume 227, ISBN 978-3-319-24098-5.
2. Seong, T.-Y.; Jung, H.; Amano, H.; Morkoc, H. *III-Nitride Based Light Emitting Diodes and Applications*, 2nd ed.; Springer: Dordrecht, The Netherlands, 2017; Volume 133, ISBN 978-981-10-3754-2.
3. Würtele, M.A.; Kolbe, T.; Lipsz, M.; Külberg, A.; Weyers, M.; Kneissl, M.; Jekel, M. Application of GaN-based ultraviolet-C light emitting diodes—UV LEDs—For water disinfection. *Water Res.* **2011**, *45*, 1481–1489. [[CrossRef](#)] [[PubMed](#)]
4. Vilhunen, S.; Särkkä, H.; Sillanpää, M. Ultraviolet light-emitting diodes in water disinfection. *Environ. Sci. Pollut. Res.* **2009**, *16*, 439–442. [[CrossRef](#)] [[PubMed](#)]
5. Kneissl, M.; Seong, T.Y.; Han, J.; Amano, H. The emergence and prospects of deep-ultraviolet light-emitting diode technologies. *Nat. Photonics* **2019**, *13*, 233–244. [[CrossRef](#)]
6. Takano, T.; Mino, T.; Sakai, J.; Noguchi, N.; Tsubaki, K.; Hirayama, H. Deep-ultraviolet light-emitting diodes with external quantum efficiency higher than 20% at 275 nm achieved by improving light-extraction efficiency. *Appl. Phys. Express* **2017**, *10*, 031002. [[CrossRef](#)]
7. Zhang, J.; Zhao, H.; Tansu, N. Effect of crystal-field split-off hole and heavy-hole bands crossover on gain characteristics of high Al-content AlGaIn quantum well lasers. *Appl. Phys. Lett.* **2010**, *97*, 111105. [[CrossRef](#)]

8. Liu, C.; Zhang, J. Influence of quantum well design on light polarization switching in AlGa_N ultraviolet emitters. *AIP Adv.* **2018**, *8*, 085125. [[CrossRef](#)]
9. Zhang, J.; Zhao, H.; Tansu, N. Large optical gain AlGa_N-delta-GaN quantum wells laser active regions in mid- and deep-ultraviolet spectral regimes. *Appl. Phys. Lett.* **2011**, *98*, 171111. [[CrossRef](#)]
10. Liu, C.; Ooi, Y.K.; Zhang, J. Proposal and physics of AlInN-delta-GaN quantum well ultraviolet lasers. *J. Appl. Phys.* **2016**, *119*, 083102. [[CrossRef](#)]
11. Zhang, J.; Tansu, N. Engineering of AlGa_N-delta-GaN quantum-well gain media for mid- and deep-ultraviolet lasers. *IEEE Photonics J.* **2013**, *5*, 2. [[CrossRef](#)]
12. Saifaddin, B.K.; Almogbel, A.; Zollner, C.J. Fabrication technology for high light- extraction ultraviolet thin-film flip-chip (UV TFFC) LEDs grown on SiC. *Semicond. Sci. Technol.* **2019**, *34*, 035007. [[CrossRef](#)]
13. Saifaddin, B.K.; Almogbel, A.S.; Zollner, C.J.; Wu, F.; Bonef, B.; Iza, M.; Nakamura, S.; Denbaars, S.P.; Speck, J.S. AlGa_N Deep-Ultraviolet Light-Emitting Diodes Grown on SiC Substrates. *ACS Photonics* **2020**, *7*, 554–561. [[CrossRef](#)]
14. Grandusky, J.R.; Gibb, S.R.; Mendrick, M.C.; Moe, C.; Wraback, M.; Schowalter, L.J. High output power from 260 nm Pseudomorphic ultraviolet light-emitting diodes with improved thermal performance. *Appl. Phys. Express* **2011**, *4*, 082101. [[CrossRef](#)]
15. Grandusky, J.R.; Chen, J.; Gibb, S.R.; Mendrick, M.C.; Moe, C.G.; Rodak, L.; Garrett, G.A.; Wraback, M.; Schowalter, L.J. 270 nm Pseudomorphic ultraviolet light-emitting diodes with over 60 mW continuous wave output power. *Appl. Phys. Express* **2013**, *6*, 032101. [[CrossRef](#)]
16. Liu, D.; Cho, S.J.; Park, J.; Seo, J.H.; Dalmau, R.; Zhao, D.; Kim, K.; Gong, J.; Kim, M.; Lee, I.K.; et al. 229 nm UV LEDs on aluminum nitride single crystal substrates using p-type silicon for increased hole injection. *Appl. Phys. Lett.* **2018**, *112*, 081101. [[CrossRef](#)]
17. Zhao, H.; Liu, G.; Tansu, N. Analysis of InGa_N-delta-InN quantum wells for light-emitting diodes. *Appl. Phys. Lett.* **2010**, *97*, 131114. [[CrossRef](#)]
18. Verma, J.; Kandaswamy, P.K.; Protasenko, V.; Verma, A.; Grace Xing, H.; Jena, D. Tunnel-injection Ga_N quantum dot ultraviolet light-emitting diodes. *Appl. Phys. Lett.* **2013**, *102*, 041103. [[CrossRef](#)]
19. Verma, J.K.; Protasenko, V.V.; Islam, S.M.; Xing, H.; Jena, D. Boost in deep-UV electroluminescence from tunnel-injection Ga_N/Al_N quantum dot LEDs by polarization-induced doping. In Proceedings of the SPIE OPTO—Gallium Nitride Materials and Devices IX, San Francisco, CA, USA, 1–6 February 2014; Volume 8986.
20. Islam, S.M.; Protasenko, V.; Lee, K.; Rouvimov, S.; Verma, J.; Xing, H.; Jena, D. Deep-UV emission at 219 nm from ultrathin MBE Ga_N/Al_N quantum heterostructures. *Appl. Phys. Lett.* **2017**, *111*, 091104. [[CrossRef](#)]
21. Islam, S.M.; Protasenko, V.; Rouvimov, S.; Xing, H.G.; Jena, D. Sub-230 nm deep-UV emission from Ga_N quantum disks in Al_N grown by a modified Stranski—Krastanov mode. *Jpn. J. Appl. Phys.* **2016**, *55*, 05FF06. [[CrossRef](#)]
22. Taniyasu, Y.; Kasu, M. Polarization property of deep-ultraviolet light emission from C-plane Al_N/Ga_N short-period superlattices. *Appl. Phys. Lett.* **2011**, *99*, 251112. [[CrossRef](#)]
23. Liu, C.; Ooi, Y.K.; Islam, S.M.; Xing, H.G.; Jena, D.; Zhang, J. 234 nm and 246 nm Al_N-Delta-GaN quantum well deep ultraviolet light-emitting diodes. *Appl. Phys. Lett.* **2018**, *112*, 011101. [[CrossRef](#)]
24. Liu, C.; Ooi, Y.K.; Islam, S.M.; Verma, J.; Xing, H.; Jena, D.; Zhang, J. Physics and polarization characteristics of 298 nm Al_N-delta-GaN quantum well ultraviolet light-emitting diodes. *Appl. Phys. Lett.* **2017**, *110*, 071103. [[CrossRef](#)]
25. Liu, C.; Lee, K.; Islam, S.M.; Xing, H.; Jena, D.; Zhang, J. Demonstration of AlGa_N-delta-GaN QW by plasma-assisted molecular beam epitaxy for 260-nm ultraviolet light emitting diodes. In Proceedings of the SPIE OPTO—Gallium Nitride Materials and Devices XIII, San Francisco, CA, USA, 27 January–1 February 2018; Volume 10532.
26. Liu, C.; Lee, K.; Harden, G.; Hoffman, A.; Xing, H.G.; Jena, D.; Zhang, J. High Internal Quantum Efficiency from AlGa_N-delta-GaN Quantum Well at 260 nm. In Proceedings of the Conference on Lasers and Electro-Optics, Washington, DC, USA, 10–15 May 2020; p. AF11.2.
27. Zhao, H.; Arif, R.A.; Ee, Y.K.; Tansu, N. Self-consistent analysis of strain-compensated InGa_N-AlGa_N quantum wells for lasers and light-emitting diodes. *IEEE J. Quantum Electron.* **2009**, *45*, 66. [[CrossRef](#)]
28. Chuang, S.; Chang, C. k-p method for strained wurtzite semiconductors. *Phys. Rev. B Condens. Matter Mater. Phys.* **1996**, *54*, 2491. [[CrossRef](#)] [[PubMed](#)]

29. Chuang, S.L.; Chang, C.S. A band-structure model of strained quantum-well wurtzite semiconductors. *Semicond. Sci. Technol.* **1997**, *12*, 252. [[CrossRef](#)]
30. Chuang, S.L. Optical gain of strained wurtzite GaN quantum-well lasers. *IEEE J. Quantum Electron.* **1996**, *32*, 1791. [[CrossRef](#)]
31. Chuang, S.L. *Physics of Photonic Devices*; John Wiley & Sons: Hoboken, NJ, USA, 2012; ISBN 9780470293195.
32. Synopsys's Optical Solutions Group. FullWAVE. Available online: <https://optics.synopsys.com> (accessed on 28 September 2020).
33. Ooi, Y.K.; Liu, C.; Zhang, J. Analysis of Polarization-Dependent Light Extraction and Effect of Passivation Layer for 230-nm AlGaIn Nanowire Light-Emitting Diodes. *IEEE Photonics J.* **2017**, *9*, 4501712. [[CrossRef](#)]
34. Ooi, Y.K.; Zhang, J. Light Extraction Efficiency Analysis of Flip-Chip Ultraviolet Light-Emitting Diodes with Patterned Sapphire Substrate. *IEEE Photonics J.* **2018**, *10*, 1–13. [[CrossRef](#)]
35. Lee, Y.J.; Kim, S.H.; Huh, J.; Kim, G.H.; Lee, Y.H.; Cho, S.H.; Kim, Y.C.; Do, Y.R. A high-extraction-efficiency nanopatterned organic light-emitting diode. *Appl. Phys. Lett.* **2003**, *82*, 3779–3781. [[CrossRef](#)]
36. Palik, E.D. *Handbook of Optical Constants of Solids*; Academic Press: Cambridge, MA, USA, 1998.
37. Zhao, H.; Liu, G.; Zhang, J.; Arif, R.A.; Tansu, N. Analysis of internal quantum efficiency and current injection efficiency in III-nitride light-emitting diodes. *IEEE/OSA J. Disp. Technol.* **2013**, *9*, 212–225. [[CrossRef](#)]
38. Shatalov, M.; Sun, W.; Lunev, A.; Hu, X.; Dobrinsky, A.; Bilenko, Y.; Yang, J.; Shur, M.; Gaska, R.; Moe, C.; et al. AlGaIn deep-ultraviolet light-emitting diodes with external quantum efficiency above 10%. *Appl. Phys. Express* **2012**, *5*, 28–31. [[CrossRef](#)]
39. Bryan, Z.; Bryan, I.; Xie, J.; Mita, S.; Sitar, Z.; Collazo, R. High internal quantum efficiency in AlGaIn multiple quantum wells grown on bulk AlN substrates. *Appl. Phys. Lett.* **2015**, *106*, 1–5. [[CrossRef](#)]
40. Shatalov, M.; Yang, J.; Sun, W.; Kennedy, R.; Gaska, R.; Liu, K.; Shur, M.; Tamulaitis, G. Efficiency of light emission in high aluminum content AlGaIn quantum wells. *J. Appl. Phys.* **2009**, *105*, 073103. [[CrossRef](#)]
41. Murotani, H.; Akase, D.; Anai, K.; Yamada, Y.; Miyake, H.; Hiramatsu, K. Dependence of internal quantum efficiency on doping region and Si concentration in Al-rich AlGaIn quantum wells. *Appl. Phys. Lett.* **2012**, *101*, 042110. [[CrossRef](#)]
42. Wang, T.Y.; Tasi, C.T.; Lin, C.F.; Wu, D.S. 85% internal quantum efficiency of 280-nm AlGaIn multiple quantum wells by defect engineering. *Sci. Rep.* **2017**, *7*, 1–8. [[CrossRef](#)] [[PubMed](#)]
43. Sun, P.; Bao, X.; Liu, S.; Ye, C.; Yuan, Z.; Wu, Y.; Li, S.; Kang, J. Advantages of AlGaIn-based deep ultraviolet light-emitting diodes with a superlattice electron blocking layer. *Superlattices Microstruct.* **2015**, *85*, 59. [[CrossRef](#)]
44. Moustakas, T.D.; Liao, Y.; Kao, C.; Thomidis, C.; Bhattacharyya, A.; Bhattarai, D.; Moldawer, A. Deep UV-LEDs with high IQE based on AlGaIn alloys with strong band structure potential fluctuations. In Proceedings of the SPIE OPTO—Light-Emitting Diodes: Materials, Devices, and Applications for Solid State Lighting XVI, San Francisco, CA, USA, 21–26 January 2012; Volume 82780.
45. Frankerl, C.; Hoffmann, M.P.; Nippert, F.; Wang, H.; Brandl, C.; Tillner, N.; Lugauer, H.J.; Zeisel, R.; Hoffmann, A.; Davies, M.J. Challenges for reliable internal quantum efficiency determination in AlGaIn-based multi-quantum-well structures posed by carrier transport effects and morphology issues. *J. Appl. Phys.* **2019**, *126*, 075703. [[CrossRef](#)]

